JCTC Journal of Chemical Theory and Computation

Efficient Structure Optimization with Second-Order Many-Body Perturbation Theory: The RIJCOSX-MP2 Method

Simone Kossmann[†] and Frank Neese*[,†,‡]

Institut für Physikalische und Theoretische Chemie, Universität Bonn, Wegelerstrasse 12, D-53115 Bonn, Germany and Max-Planck Institut für Bioanorganische Chemie, Stiftstrasse 34−36, D-45470 Mülheim an der Ruhr, Germany

Received April 14, 2010

Abstract: Efficient energy calculations and structure optimizations employing second-order Møller−Plesset perturbation theory (MP2) are presented. The application of the RIJCOSX approximation, which involves different approximations for the formation of the Coulomb- and exchange-type matrices, to MP2 theory is demonstrated. The RIJCOSX approximation incorporates the 'resolution of the identity' approximation in terms of a Split-RI-J variant for the evaluation of the Coulomb matrices and a seminumeric exchange treatment via the 'chain-of-spheres' algorithm for the formation of the exchange-type matrices. Beside the derivation of the working equations, the RIJCOSX-MP2 method is benchmarked against the original MP2 and the already highly efficient RI-MP2 method. Energies as well as gradients are computed employing various basis sets and are compared to the conventional MP2 results concerning accuracy and total wall clock times. Speedups of typically a factor of 5−7 in comparison to MP2 can be obeserved for the largest basis set employed in our study. Total energies are reproduced with an average error of ≤0.8 kcal/mol and minimum energy geometries differ by ∼0.1 pm in bond lengths and typically ∼0.2 degrees in bond angles. The RIJCOSX-MP2 gradient parallelizes with a speedup of 8.2 on 10 processors. The algorithms are implemented into the ORCA electronic structure package.

Introduction

Second-order many-body perturbation theory (MBPT2) with the Møller−Plesset partitioning of the Hamiltonian (MP2)[1] is the simplest ab initio method that accounts for dynamic electron correlation effects. MP2 theory has proven to be a great improvement over Hartree−Fock (HF) theory and is therefore widely used in computational chemistry. Besides its formal simplicity MP2 features, few elementary properties: (a) MP2 is size extensive but only size consistent when based on a size consistent reference wave function, (b) MP2 recovers 80−90% of the basis set correlation energy, (c) MP2 scales only with $\mathcal{O}(N^5)$, and (d) MP2 based on a HF reference wave function only contains double excitation amplitudes.

The shortcomings of MP2 theory are also well-known, i.e., MP2 is not variational or even stationary with respect to wave function parameters, and it does not incorporate any orbital relaxation when based on a HF reference determinant. Orbital relaxation is partially taken into account, if Brillouins' theorem[2] no longer applies, and single excitations contribute to the first-order wave function. The nonvariational character of MP2 is of minor consequence for the calculation of electron correlation effects but complicates and increases the computational effort for the computation of MP2 derivatives.

In the last two decades many attempts have been undertaken in the improvement of the quality and efficiency of MP2 calculations. On the one hand, empirical parameters have been determined to individually scale the parallel and

* Corresponding author. E-mail: theochem@thch.uni-bonn.de.
[†] Universität Bonn.
[‡] Max-Planck Institut für Bioanorganische Chemie.

10.1021/ct100199k
Published on Web 07/02/2010

antiparallel spin components in MP2 theory, e.g., Grimme's 'spin-component scaled' MP2 (SCS-MP2)[3,4] or the simplified approach of Head-Gordon et al. 'scaled opposite-spin' MP2 (SOS-MP2)[5−7] that also leads to reduced computational scaling from $\mathcal{O}(N^5)$ to $\mathcal{O}(N^4)$. On the other hand, the development of double-hybrid functionals has introduced semilocal dynamic correlation effects by adding a perturbative second-order correction in the framework of density functional theory.[8,9]

Substantial progress to improve the efficiency of MP2 calculations was made by Almlöf and Saebo by introducing an integral direct MP2 algorithm to avoid storage of $\mathcal{O}(N^4)$ intermediates.[10] Further modifications to the original algorithm have been reported by Head-Gordon and Pople[11] as well as by Ahlrichs.[12] Probably, the most efficient semidirect ansatz, without avoiding the storage of $\mathcal{O}(N^4)$ quantities on disk, was proposed by Pulay and co-workers,[13−16] who presented very large MP2 calculations with more than 2000 basis functions.[17] A linear scaling integral direct MP2 code based on the Laplace transformation technique introduced by Almlöf,[18] and discussed by various authors,[19−21] has been developed by Ochsenfeld and co-workers.[22−25] Among others Werner, Schütz, and co-workers have developed efficient approximate linear scaling approaches[26−30] which employed the correlation domain concept of Pulay and Saebo.[31−33] The most popular approximation used in combination with the MP2 method is the 'resolution of the identity' (RI) approximation, in which products of orbitals are expanded in an auxiliary basis set.[34] The RI-MP2 method was first reported by Feyereisen et al.[35] and was based on the results of Vahtras, Feyereisen, and Almlöf who showed that the RI technique performs best in the Coulomb metric.[36] The outstanding performance of the RI-MP2 method is indisputable. The speedup of one to two orders of magnitude for large basis sets in comparison to the canonical result with errors in energies usually smaller than 0.1 mE_h/atom demonstrates the impressive efficiency of the RI-MP2 method.

The first derivation and implementation of the MP2 gradient was reported by Pople at the end of the 1970s.[37] Direct and semidirect variants of the MP2 gradient implementation have been developed by Frisch, Head-Gordon, and Pople more than 10 years later.[38,39] Ahlrichs implemented a modification of the semidirect MP2 gradient with reduced disk storage requirements and the exploit of nonabelian point group symmetry in the well-know MPGRAD program that is part of the TuboMole program suite.[12]

Weigend and Häser demonstrated the efficient use of the RI approximation in MP2 gradient calculations.[40] Further refinement was made by Head-Gordon and co-workers who first presented the restricted open-shell MP2 gradient within the RI approximation[41] and later on proposed a more efficient RI-MP2 gradient algorithm by utilizing a semidirect batching approach.[42] Analytic derivatives associated with the recently developed double-hybrid functionals have been reported by Neese, Schwabe, and Grimme,[9] who also demonstrated the efficient application of the RI approximation to the incorporated MP2 correction.

Like any other wave function-based electron correlation theory, the basis set requirements for MP2 calculations are much more stringent than for self-consistent field (SCF) calculations. Hence, in order to obtain results that properly reflect the intrinsic accuracy of the MP2 method rather than basis set incompleteness artifacts, one needs to employ at least a triple-ζ basis with at least two or three sets of polarization functions.[43] However, in order to obtain truly converged results much larger basis sets are necessary. Fortunately, basis set extrapolation techniques are known that allow one to extrapolate to the MP2 basis set limit. However, the preferred level for a reliable extrapolation still involves triple- and quadruple-ζ basis sets. In this case, traditional SCF and MP2 calculations become very expensive and highly time consuming. Thus, it is desirable to search for algorithms that perform efficiently with such extended basis sets for at least medium-sized molecules that are described by 500−2000 basis functions. In this respect, the RI-MP2 method is a great achievement since it performs much better than the standard MP2 algorithms for extended basis sets. In fact, in calculations with extended basis sets the SCF calculation, despite its more favorable computational scaling, usually strongly dominates over the RI-MP2 step in terms of execution time. We have recently shown that great speedups by up to an order of magnitude can be obtained with negligible loss of accuracy, if the SCF step is performed in an approximate way that involves the RI approximation for the Coulomb integrals, while performing a semianalytic integration of the exchange term in the HF equations.[44] This concept can be easily adopted for RI-MP2 energy calculations, since the employed approximations to the HF equations do not enter the familiar calculation of the RI-MP2 energy correction. The seminumeric algorithm used to approximate the exchange term is called 'chain of spheres' (COSX), hence, this algorithm is termed RIJCOSX-MP2. COSX is closely related to Friesners pioneering pseudospectral techniques but is conceptually simpler, as discussed in detail in ref 44. In this manuscript we extend this concept to the first derivatives of the RIJCOSX-MP2 energy. Substantial savings compared to the standard MP2 and the RI-MP2 methods arise from the more efficient SCF step, the more efficient treatment of derivative integrals in the atomic orbital (AO) basis, and the accelerated solution of the z-vector equations.[45] We emphasize that the computational savings immediatly carry over to the case of double-hybrid density functional theory that inherits from RI-MP2 the significant basis set dependence.

Theory

In this section, the theory of the RI-MP2 gradient in the RIJCOSX-MP2 approximation is described in some detail. Throughout this paper, indices i, j, k, ... refer to occupied orbitals in the Hartree−Fock reference determinant, a, b, c, ... to virtual orbitals, and p, q, r, ... to general orbitals from either set. Capital letters denote auxiliary basis functions, whereas K, L, M, and N assign basis functions from the Coulomb-fitting basis sets and R, S, T, and U indicate optimized basis functions for the RI treatment of the correlation correction. Greek letters μ, ν, κ, ... refer to atomic basis functions.

Seminumeric Exchange Matrix. We briefly review the seminumerical exchange treatment that is efficiently implemented in the ORCA program package within the 'chain of spheres' algorithm (COSX).[44] The basic idea for the efficient evaluation of exchange-type matrices is to combine a numeric integration in the physical space with an analytic integration over the Coulomb singularity.

The conventional exchange-type matrix is given as

$$K_{\mu\nu} = \sum_{\kappa\tau} P_{\kappa\tau}(\mu\kappa|\nu\tau) \tag{1}$$

where $P_{\kappa\tau}$ is any density-type matrix and $(\mu\kappa|\nu\tau)$ is a two-electron repulsion integral over atomic basis functions $\{\varphi\}$.

The exchange integrals can be approximated as

$$\begin{aligned}(\mu\kappa|\nu\tau) &= \int d\mathbf{r}'\varphi_\mu(\mathbf{r}')\varphi_\kappa(\mathbf{r}')\int d\mathbf{r}\frac{\varphi_\nu(\mathbf{r})\varphi_\tau(\mathbf{r})}{|\mathbf{r}-\mathbf{r}'|} \\ &\approx \sum_g w_g\varphi_\mu(\mathbf{r}_g)\varphi_\kappa(\mathbf{r}_g)\int d\mathbf{r}\frac{\varphi_\nu(\mathbf{r})\varphi_\tau(\mathbf{r})}{|\mathbf{r}-\mathbf{r}_g|}\end{aligned} \tag{2}$$

where the first analytical integration over the coordinates $\mathbf{r}'$ is replaced by a numerical integration over grid points $\mathbf{r}_g$. The corresponding grid weights w_g are determined by Becke's weighting scheme.[46] The exchange-type matrix can then be efficiently evaluated as,

$$K_{\mu\nu} \approx \sum_g X_{\mu g}\sum_\tau A_{\nu\tau}(\mathbf{r}_g)\sum_\kappa X_{\kappa g}P_{\kappa\tau} \tag{3}$$

with

$$X_{\mu g} = w_g^{1/2}\varphi_\mu(\mathbf{r}_g) \tag{4}$$

$$A_{\nu\tau}(\mathbf{r}_g) = \int \frac{\varphi_\nu(\mathbf{r})\varphi_\tau(\mathbf{r})}{|\mathbf{r}-\mathbf{r}_g|}d\mathbf{r} \tag{5}$$

We further define

$$F_{\tau g} = \sum_\kappa P_{\kappa\tau}X_{\kappa g} \tag{6}$$

$$G_{\nu g} = \sum_\tau F_{\tau g}A_{\nu\tau}(\mathbf{r}_g) \tag{7}$$

As mentioned in the Introduction, these equations are closely related to Friesners pseudospectral method. However, there a least-squares fitting operator $Q_{\kappa g}$ is used that is simply replaced by $X_{\kappa g}$ in our formulation. The connection between the COSX and pseudospectral methods is discussed in detail in ref 47.

The exchange energy can be evaluated as

$$E_X = \sum_{\mu\nu} tr(\mathbf{FG}^+)_{\mu\nu} \tag{8}$$

Seminumeric Exchange Gradient. The exchange gradient can be written as

$$\frac{\partial K_{\mu\nu}}{\partial\lambda} = \sum_{\kappa\tau} P_{\kappa\tau}\frac{\partial(\mu\kappa|\nu\tau)}{\partial\lambda} \tag{9}$$

Due to the permutational symmetry of the exchange integrals, the derivative expression can be rearranged as follows

$$\sum_{\kappa\tau} P_{\kappa\tau}(\mu\kappa|\nu\tau^\lambda) \approx \sum_g X_{\mu g}\sum_\tau A_{\nu\tau^\lambda}(\mathbf{r}_g)\sum_\kappa X_{\kappa g}P_{\kappa\tau} \tag{10}$$

$$= \sum_{\kappa\tau} P_{\kappa\tau}(\nu\tau^\lambda|\mu\kappa) \approx \sum_g X_{\nu g}\sum_\kappa A_{\mu\kappa}(\mathbf{r}_g)\sum_\tau X_{\tau^\lambda g}P_{\kappa\tau} \tag{11}$$

where $X_{\tau^\lambda g}$ is defined by

$$X_{\tau^\lambda g} = w_g^{1/2}\frac{\partial\varphi_\tau(\mathbf{r}_g)}{\partial\lambda} \tag{12}$$

The formulation of the exchange gradient differs only slightly from the derivation of the seminumeric exchange itself. Due to the rearrangement of the two-electron exchange gradient integrals, only the derivatives of the basis functions on the grid are needed instead of the derivatives of the analytic integrals.

Density Fitting. The Coulomb matrix can be efficiently approximated by expanding products of basis functions in an extended auxiliary basis set that is usually two to four times larger than the orbital basis set.[36,48,49] The variant of this method that is used in the ORCA program is called 'Split-RI-J' and is described in ref 50.

In terms of the RI approximation, the Coulomb matrix is given as

$$J_{\mu\nu} \approx \sum_K d_K(\mu\nu|K) \tag{13}$$

With the three-index two-electron repulsion integral:

$$(\mu\nu|K) = \int \mu(\mathbf{r}_1)\nu(\mathbf{r}_1)r_{12}^{-1}K(\mathbf{r}_2)d\mathbf{r}_1d\mathbf{r}_2 \tag{14}$$

where $K(\mathbf{r}_2)$ is a member of the auxiliary basis set $\{\eta\}$. The vector d_K represents the density in the auxiliary basis which is best obtained from the linear equation system $\mathbf{Vd} = \mathbf{g}$, with $V_{KL} = (K|L)$ and $g_K = \sum_{\mu\nu}P_{\mu\nu}(\mu\nu|K)$. Feyereisen et al.[35] proposed the RI approximation for MP2 energy calculations (RI-MP2) in the mid 1990s. The MP2 energy expression within the RI framework becomes

$$E_{\mathrm{MP2}} = \frac{1}{4}\sum_{ijab}[(ia|jb) - (ib|ja)]t_{ab}^{ij} \tag{15}$$

$$E_{\mathrm{RI-MP2}} = \frac{1}{2}\sum_{iaR}(ia|R)\Gamma'^R_{ai} \tag{16}$$

where we defined the three-index two-particle density as $\Gamma'^R_{ai} = \sum_{jbS}V_{RS}^{-1}(S|bj)t_{ab}^{ij}$. The RI-MP2 double excitation amplitudes t_{ab}^{ij} are given as

$$t_{ab}^{ij} = -\sum_{RS}\frac{(ia|R)V_{RS}^{-1}(S|jb) - (ib|R)V_{RS}^{-1}(S|ja)}{\varepsilon_a + \varepsilon_b - \varepsilon_i - \varepsilon_j} \tag{17}$$

RI-MP2 Gradient. The RI-MP2 gradient is efficiently calculated employing the RI approximation.[40] The general RI-MP2 gradient expression written in AO basis is

$$E_2^\lambda = \sum_{\mu\nu} D_{\mu\nu} h_{\mu\nu}^\lambda + \sum_{\mu\nu} W_{\mu\nu} S_{\mu\nu}^\lambda + \sum_{\mu\nu\kappa\tau} \Gamma_{\mu\nu\kappa\tau}^S (\mu\nu|\kappa\tau)^\lambda + \Gamma_{\mu\nu\kappa\tau}^{NS} (\mu\nu|\kappa\tau)_{RI}^\lambda \quad (18)$$

where $D_{\mu\nu}$ denotes the relaxed MP2 density, $W_{\mu\nu}$ is the energy weighted density matrix, and $\Gamma_{\mu\nu\kappa\tau}$ indicates the separable ('S') and nonseparable ('NS') part of the two-particle density matrix. The separable fraction of the two-particle density matrix contains products of the SCF and MP2 density matrices, whereas the nonseparable contribution consists of the MP2 double excitation amplitudes. While $h_{\mu\nu}^\lambda$ denotes the derivative of the one-electron operator and the corresponding basis functions with respect to nuclear displacements $\lambda = x$, y, and z, $S_{\mu\nu}^\lambda$ is the derivative of the overlap matrix, and $(\mu\nu|\kappa\tau)^\lambda$ represents the derivative of the two-electron repulsion integrals with or without the RI approximation.

The relaxed MP2 density matrix is defined as

$$D_{\mu\nu} = \sum_{pq} c_{\mu p} c_{\nu q} D_{pq} \quad (19)$$

$$D_{ij} = -\frac{1}{2} \sum_{kab} t_{ab}^{ik} t_{ab}^{jk} \quad (20)$$

$$D_{ab} = \frac{1}{2} \sum_{ijc} t_{ac}^{ij} t_{bc}^{ij} \quad (21)$$

$$D_{ai} = D_{ia} = \frac{1}{2} z_{ai} \quad (22)$$

where z_{ai} is the solution of the 0th order z-vector equations.[45]

The coupled perturbed self-consistent field (CP-SCF) equations to be solved are $(\varepsilon_a - \varepsilon_i) z_{ai} + R(\mathbf{z})_{ai} = -L_{ai}$, with the MP2 Lagrangian given by

$$L_{ai} = 2 \sum_{cR} (ac|R) \Gamma'^R_{ic} - 2 \sum_{kR} (ki|R) \Gamma'^R_{ka} + R(\mathbf{D})_{ai} \quad (23)$$

The response operator $R(\mathbf{P})_{pq}$ in the AO basis is defined in a general way as

$$R(\mathbf{P})_{\mu\nu} = \sum_{\kappa\tau} P_{\kappa\tau} (2(\mu\nu|\kappa\tau) - (\mu\tau|\kappa\nu) - (\nu\tau|\kappa\mu)) \quad (24)$$

where $\mathbf{P}$ denotes any density-type matrix.

The energy weighted density matrix incorporates all terms that have to be contracted with the derivative of the overlap matrix:

$$W_{\mu\nu} = \sum_{pq} c_{\mu p} c_{\nu q} W_{pq} \quad (25)$$

$$W_{ij} = -\sum_{aR} (ja|R) \Gamma'^R_{ia} - \frac{1}{2} D_{ij} (\varepsilon_i + \varepsilon_j) - \frac{1}{2} R(\mathbf{D})_{ij} \quad (26)$$

$$W_{ab} = -\sum_{iR} (ib|R) \Gamma'^R_{ia} - \frac{1}{2} D_{ab} (\varepsilon_a + \varepsilon_b) \quad (27)$$

$$W_{ai} = -2 \sum_{kR} (ki|R) \Gamma'^R_{ka} - D_{ai} \varepsilon_i \quad (28)$$

Finally, the last two terms in eq 18 contain the derivative of the non-RI and RI two-electron repulsion integrals with respect to nuclear displacements:

$$\Gamma_{\mu\nu\kappa\tau}^S (\mu\nu|\kappa\tau)^\lambda = (D_{\mu\nu} P_{\kappa\tau}^{SCF} - D_{\mu\kappa} P_{\nu\tau}^{SCF}) (\mu\nu|\kappa\tau)^\lambda \quad (29)$$

$$\Gamma_{\mu\nu\kappa\tau}^{NS} (\mu\nu|\kappa\tau)_{RI}^\lambda = \sum_{ijab} c_{\mu i} c_{\nu a} c_{\kappa j} c_{\tau b} t_{ab}^{ij} \times \left[\sum_{RS} \{ (\mu\nu|R)^\lambda V_{RS}^{-1} (S|\kappa\tau) + (\mu\nu|R) V_{RS}^{-1} (S|\kappa\tau)^\lambda \} - \sum_{RSTU} (\mu\nu|T) V_{TR}^{-1} V_{RS}^\lambda V_{SU}^{-1} (U|\kappa\tau) \right] \quad (30)$$

RIJCOSX-MP2 Gradient. The RIJCOSX algorithm combines the seminumeric exchange treatment for all exchange terms with the RI approximation for all Coulomb-type contributions. The total RIJCOSX-MP2 energy is calculated as

$$\begin{aligned} E_{\text{RIJCOSX-MP2}} &= E_{\text{RIJCOSX-HF}} + E_{\text{RI-MP2}} \\ &= \sum_{\mu\nu} P_{\mu\nu} h_{\mu\nu} + \frac{1}{2} \sum_{\mu\nu} P_{\mu\nu} \sum_{\kappa\tau} P_{\kappa\tau} \times \sum_{KL} (\mu\nu|K) V_{KL}^{-1} (L|\kappa\tau) \\ &\quad - \frac{1}{2} \sum_{\mu\nu} P_{\mu\nu} \sum_g X_{\mu g} \sum_\tau A_{\nu\tau}(\mathbf{r}_g) \sum_\kappa X_{\kappa g} P_{\kappa\tau} \\ &\quad + \frac{1}{2} \sum_{\mu\nu R} (\mu\nu|R) \Gamma'^R_{\mu\nu} \end{aligned} \quad (31)$$

Thus, the RIJCOSX-MP2 energy correction corresponds to the original RI-MP2 energy correction, and the unrelaxed MP2 difference density is calculated as in the standard RI-MP2 formulation. The COSX approximation enters into the SCF energy and then into the evaluation of the response-type operators (eq 24) required for the construction of the Lagrangian (eq 23) as well as the internal part of the energy weighted density matrix in eq 26.

For the calculation of the response operator, the Coulomb-type two-electron integral is evaluated employing the RI approximation, whereas both exchange-type integrals are calculated using the COSX algorithm. Thus, the RIJCOSX response-type operator is approximated as

$$\begin{aligned} R(\mathbf{P})_{\mu\nu} \approx & \sum_{\kappa\tau} P_{\kappa\tau} \left(2 \sum_{KL} (\mu\nu|K) V_{KL}^{-1} (L|\kappa\tau) \right) - \\ & \sum_g X_{\mu g} \sum_\kappa A_{\kappa\nu}(\mathbf{r}_g) \sum_\tau X_{\tau g} P_{\kappa\tau} - \sum_g X_{\nu g} \sum_\kappa A_{\kappa\mu}(\mathbf{r}_g) \sum_\tau X_{\tau g} P_{\kappa\tau} \end{aligned} \quad (32)$$

In this way, all exchange- and Coloumb-type two-electron integrals occurring in the Fock and response operators are evaluated in the SCF and CP-SCF procedures.

In the RIJCOSX treatment, the derivatives of the basis functions with respect to nuclear replacements are contracted with the separable part of the two-particle density matrix (eq 29) as follows

$$\begin{aligned}\Gamma^{S}_{\mu\nu\kappa\tau}(\mu\nu|\kappa\tau)^{\lambda} &= D_{\mu\nu}P^{\mathrm{SCF}}_{\kappa\tau}((\mu\nu|\kappa\tau)^{\lambda} - (\mu\kappa|\nu\tau)^{\lambda}) \\ &= D_{\mu\nu}P^{\mathrm{SCF}}_{\kappa\tau}[2\sum_{KL}(\mu\nu|K)^{\lambda}V^{-1}_{KL}(L|\kappa\tau) - \\ &\quad \sum_{KLMN}(\mu\nu|M)V^{-1}_{MK}V^{\lambda}_{KL}V^{-1}_{LN}(N|\kappa\tau)] \\ &\quad + 2\sum_{g}\sum_{\mu\nu}\frac{\partial F^{\mathrm{SCF}}_{\mu g}}{\partial\lambda}G^{\mathrm{MP2}}_{\nu g} \\ &\quad + 2\sum_{g}\sum_{\mu\nu}\frac{\partial F^{\mathrm{MP2}}_{\mu g}}{\partial\lambda}G^{\mathrm{SCF}}_{\nu g}\end{aligned} \tag{33}$$

where the superscripts SCF and MP2 indicate either the SCF density matrix or the MP2 difference density matrix with

$$\frac{\partial F_{\mu g}}{\partial\lambda} = \sum_{\kappa}P_{\mu\kappa}X_{\mu^{\lambda}g} \tag{34}$$

The seminumeric MP2 exchange gradient is implemented, as shown in Figure 1. The first step is to obtain the basis functions and its derivatives on the grid and to scale them with its corresponding weighting factor. Then the 'Batch-Density' is constructed as contraction of the density matrix elements that correspond to nonzero basis function values. $F_{\mu g}$ and the derivatives $F^{\lambda}_{\mu g}$ are calculated with the SCF density matrix as well as with the MP2 density matrix, where λ corresponds to the three Cartesian coordinates. The $F_{\mu g}$ terms are required for the calculation of the exchange energy, see eq 8. After the calculation of the intermediate $G_{\nu g}$, the three components of the gradient can be evaluated as presented in Figure 1. Since we allow for different auxiliary basis sets to approximate the Coulomb-type matrices (/J) and the MP2 exchange operators (/C), all terms that originate from the HF and coupled-perturbed HF equations are calculated with the smaller *J*-auxbasis set, indicated by labels *K*, *L*, *M*, and *N*. These terms are the Coulomb-type terms in the RIJCOSX-HF energy and in the response operator (eq 24) as well as the derivative Coulomb integrals contracted with the separable part of the two-electron density (eq 33). By contrast, the three-index integrals for the evaluation of the RI-MP2 energy correction and the derivative Coulomb integrals that are contracted with the nonseparable density have to be approximated by employing the *C*-auxbasis set, denoted by indices *R*, *S*, *T*, and *U*.

Calculations

Computational Details. All calculations were performed with a development version of the ORCA program package.[51] The split-valence ((def2-)SV),[52] triple-ζ valence ((def2-)TZV),[53] and quadruple-ζ valence ((def2-)QZV)[54] basis sets developed by the Karlsruhe group together with the appropriate polarization functions from the TurboMole library were used throughout.[55] In order to obtain optimum results, different auxiliary basis sets should be used for the approximation of the Coulomb term[56] and the MP2 energy[57−60] (/J and /C in ORCA notation, respectively). Alternatively, the larger Coulomb plus exchange[61] (/JK in ORCA notation) auxiliary basis sets can be used for the entire calculation, although the MP2 energies obtained with these fitting bases are noticeably inferior to the ones obtained with the C-bases. Nevertheless, the noncompleteness errors in the RI approximation are so smooth that the choice of auxiliary basis set does play a minor role for chemical applications, and an unbalanced or erroneous behavior was never observed with any of the tested auxiliary basis sets.

```
Calculate the basis function φ and its derivatives φ^λ on the grid
Scale φ and φ^λ with w_g^½
Loop over number of input densities
  Construct BatchDensity matrix P^SCF and P^MP2
  Calculate F^SCF_μg ⇐ P^SCF ⋆ φ and F^MP2_μg ⇐ P^MP2 ⋆ φ
  Calculate F^SCF,λ_μg ⇐ P^SCF ⋆ φ^λ and F^MP2,λ_μg ⇐ P^MP2 ⋆ φ^λ, λ = x, y, z
End loop over number of input densities
Calculate G^SCF_νg and G^MP2_νg
Calculate GRAD^λ[atom] ⇐ tr(F^SCF,λ G^MP2†_νg) + tr(F^MP2,λ G^SCF†_νg)
```

Figure 1. Pseudocode for the implementation of the separable COSX-MP2 gradient.

Calculations labeled RI-MP2 used the RI[36] approximation only for the calculation of the MP2 correction. In RIJ-DX-MP2 calculations exact analytic integration of the exchange contribution and the RI approximation for the Coulomb terms were employed. The label RIJCOSX-MP2 refers to a RI-MP2 calculation where the COSX approximation[44] in conjunction with Split-RI-J[50] (in the SCF part), and the standard RI approximation (in the MP2 part) was employed. In RIJCOSX-MP2 calculations the default SCF grids[44] were used to obtain the HF energy. For the calculation of the response operator (eq 24) and for the solution of the *z*-vector equations, a Lebedev-50 angular integration grid with an integration accuracy of 3.34 has been determined to be sufficient in extended test calculations. However, for the calculation of the derivatives of the basis functions on the grid (eq 12), a large Lebedev-302 angular grid with a radial integration accuracy of 4.34 is required to prevent the buildup of numerical noise.

Total energies were generally converged to 10^{-8} E_{h}. To benchmark the optimized structures, energy convergence tolerances of 10^{-10} E_h and tight optimization criteria were enforced. The frozen-core approximation[62] was employed throughout, and the time savings compared to the all-electron treatment are ~10% for the RIJCOSX-MP2 treatment, determined on the example of the D-glucose molecule in combination with the TZVPP or QZVP basis set.

Integration Grids. The integration grids employed for the numerical integration within the COSX algorithm were derived from standard density functional theory (DFT) grids included in the ORCA program package but are considerably smaller. The accuracy of the integration grids is controlled by the radial resolution parameter ε, which defines the number of radial shells n_r for a given atom and is calculated as $n_r = 15\varepsilon + 5r - 40$,[63] where r is the row of the periodic table to which the atom belongs. For a radial integration accuracy of $\varepsilon = \{3.34; 4.01; 4.34; 5.01\}$ the number of radial grid points for the first to third row of the periodic table is {(15,20,25); (25,30,35); (30,35,40); (40,45,50)}. The pruning algorithm of Gill et al. is used to reduce the number of points in the inner and outer regions.[64] For comparison, we have chosen the same four representative molecules with the same diverse basis sets, as for the earlier evaluation of the SCF grids.[44]

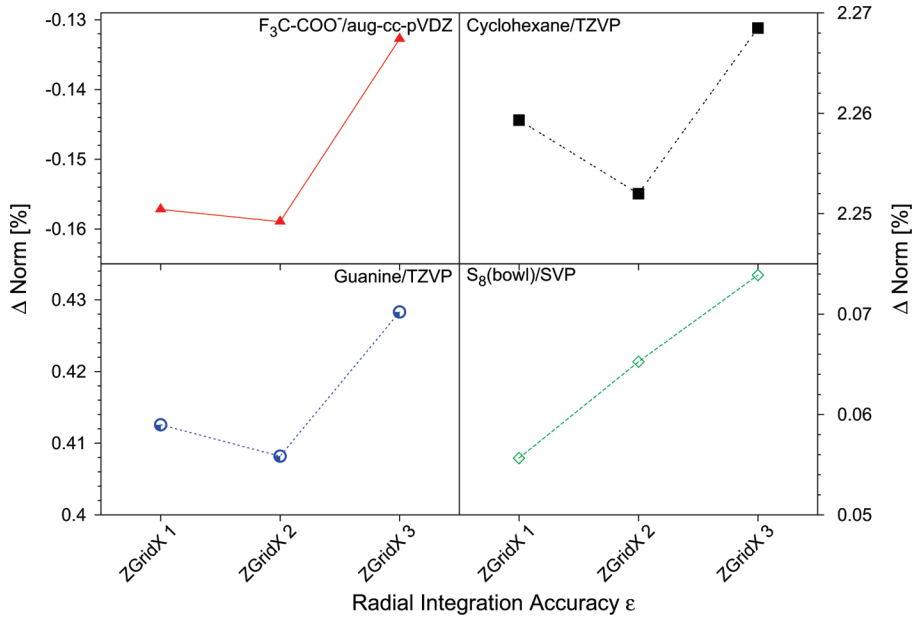

Figure 2. Deviation of the RIJCOSX-MP2 gradient norm (%) depending on the SCF grids with regard to the original MP2 method. ZGridX 1−3 refer to Lebedev-50/3.34, -50/4.01, and -194/4.34.

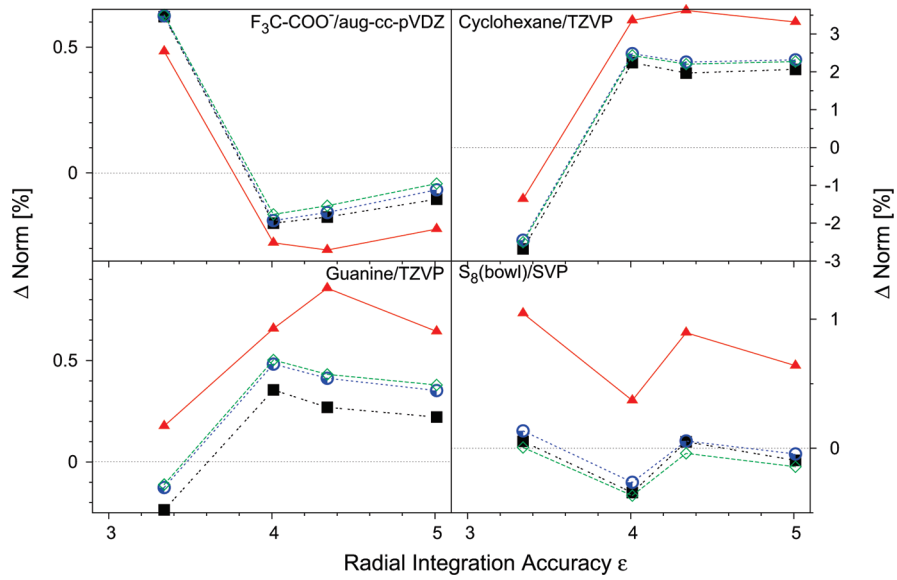

Figure 3. Deviation of the RIJCOSX-MP2 gradient norm (%) depending on the grids used for the evaluation of the basis function derivatives with regard to the original MP2 method. Triangles (▲) = 110 point, filled squares (■) = 195 point, circles (●) =302 point, and empty squares (□) = 434 point Lebedev grids.

The grids used for the calculation of the response-type operators are dependent on the chosen SCF grids, since they originate from the HF equations. Therefore, we tested the influence of the employed integration grids for the solution of the *z*-vector equations on the quality of the calculated gradient norm compared to the original MP2 gradient norm. As shown in Figure 2, the deviations of the gradient norm are very small (<3%), and the very limited deviations follow no general trend. We therefore have considered the smallest SCF grid as being appropriate for the present purpose.

The calculation of the derivative of the basis functions on the grid required for the RIJCOSX-MP2 gradient is independent of the employed SCF grids. Therefore, we tested different angular grids in combination with several radial integration accuracies. In Figure 3 the deviation of the norm calculated with the RIJCOSX approximation compared to the norm of the original MP2 method is presented.

The trend of the norm deviation changes between different molecules but is almost independent of the angular grid. The maximum deviation of the gradient norm is 3.5% for the cyclohexane molecule but is considerably smaller for the other molecules in this test suite (<1%). The curves corresponding to the large 302 and 434 point Lebedev grids nearly coincide, and even the deviations obtained with the smaller 194 point Lebedev grid are still reasonable. However, extended test calculations have shown that the best convergence in geometry optimizations is obtained with the Lebedev-302 radial grid in combination with a radial integration accuracy of 4.43. Hence, we choose this very conservative scheme as our default setting.

Table 1. Overview of the Different Approximations Employed for the SCF and MP2 Parts[a]

	approximations				
	SCF		MP2		
methods	Coulomb	exchange	correction	separable gradient	non-separable gradient
MP2 energy	exact	exact	exact	–	–
MP2 gradient	exact	exact	exact	exact	exact
RI-MP2 energy	exact	exact	RI	–	–
RI-MP2 gradient	exact	exact	RI	exact	RI
RIJ-DX-MP2 energy	RI	exact	RI	–	–
RIJ-DX-MP2 gradient	RI	exact	RI	J-RI/K-exact	RI
RIJCOSX-MP2 energy	Split-RI-J	COSX	RI	–	–
RIJCOSX-MP2 gradient	Split-RI-J	COSX	RI	J-RI/K-COSX	RI

[a] Indices J and K refer to the Coulomb and exchange contributions, respectively, RI indicates the original resolution of the identity approximation, and COSX denotes the seminumeric exchange treatment.

Table 2. Efficiency and Accuracy of the RIJ-DX and RIJCOSX Algorithms for MP2 Energy Calculations on Medium-Size Molecules with Different Basis Sets[a]

				ΔE			speedup SCF		
molecule	N_{atoms}	basis	N_{basis}	RI	RIJ-DX	RIJCOSX	RIJ-DX	RIJCOSX	speedup RI-MP2
adenine	15	TZVPP	150	0.1	−0.1	0.7	1.0	3.9	29.8
		QZVP	220	0.1	−0.1	1.1	1.0	6.9	18.7
beclometahsone	57	TZVPP	1277	0.4	−0.1	0.8	1.1	7.7	20.2
D-glucose	24	TZVPP	540	0.2	−0.2	0.0	1.1	4.5	26.3
		QZVP	1044	0.1	−0.3	0.8	1.1	7.9	21.6
dibenzo-crown-18−6	50	TZVPP	1142	0.3	−0.3	0.6	1.3	6.1	18.5
epinephrine	26	TZVPP	585	0.2	−0.2	0.5	1.1	4.4	27.2
		QZVP	1131	0.1	−0.3	1.3	1.0	7.7	24.2
menthol	31	TZVPP	621	0.2	−0.1	0.2	1.2	5.8	33.5
		QZVP	1227	0.1	−0.2	1.6	1.1	11.4	29.2
tyrosine	24	TZVPP	557	0.2	−0.1	0.6	1.1	4.9	26.0
		QZVP	1071	0.1	−0.2	1.4	1.1	7.4	22.9

[a] Speedup refers to the ratio of wall clock times of the SCF or the RI-MP2 modules (RI-MP2) required to finish one energy calculation. Speedups are given relative to the original MP2 method without any approximations. Deviation of the single point energies to the MP2 reference is denoted ΔE_{RI}, $\Delta E_{RIJ\text{-}DX}$, and $\Delta E_{RIJCOSX}$ in (kcal/mol).

Results

In this section, the RIJCOSX-MP2 method is benchmarked against the conventional MP2 as well as the RI-MP2 method in terms of accuracy and efficiency. In order to not mix up the different approximations employed, an overview of the abbreviations used is given in Table 1. Whenever the original or conventional MP2 method is mentioned, no approximations are involved. For RI-, RIJ-DX-, and RIJCOSX-MP2, the MP2 energy correction is identically calculated applying the RI approximation.

Efficiency and Accuracy of RIJCOSX-MP2 Energy Calculations. In order to demonstrate the efficiency and accuracy of the RIJCOSX approximation for MP2 energy calculations, we have calculated single point energies of seven medium-sized molecules consisting of 15−57 atoms, employing two large basis sets with up to ∼1200 basis functions. The speedups listed in Table 2 are classified in terms of speedups in the SCF calculation and in the evaluation of the MP2 correction. Due to the fact that neither the RIJ-DX nor the RIJCOSX approximation has any influence on the calculation of the RI-MP2 energy correction, the speedups displayed in the last column of Table 2 are identical for RI, RIJ-DX, and RIJCOSX. The speedups for the evaluation of the MP2 correction in terms of the RI approximation range from ∼18.5−33.5, which again demonstrates the high efficiency of the density fitting technique.

Whereas the RIJ-DX treatment represents generally no improvement over the original RI approximation, the benefit in computation time for the RIJCOSX approximation originates from the immense speedup during the SCF calculation. The HF equations in the RIJCOSX framework are solved about ∼4−11 times faster compared to that of the approximation-free RHF method. Since MP2 energy calculations are strongly dominated by the solution of the HF equations, the overall speedup that can be achieved with several approximations corresponds roughly to the speedup obtained in the SCF iterations (∼1−2 and ∼5−14 for RIJ-DX and RIJCOSX, respectively). The speedups in the SCF module are considerably lower than the speedups reported in ref 44. This is due to the fact that the integral generation package of ORCA was recently replaced with the LIBINT package designed by Valeev and Ferman that is inherently more efficient, in particular for high-angular momentum basis functions.[65] Hence, the favorable scaling of the COSX approximation with respect to higher angular momenta becomes less pronounced than previously reported. In general, the speedups obtained with the RIJCOSX approximation during the SCF iterations decrease by roughly

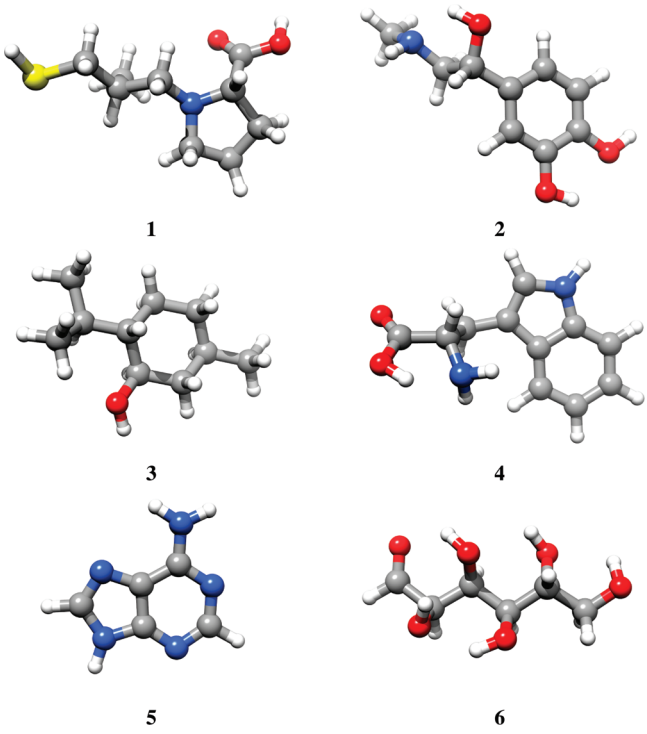

Figure 4. Systems used for testing the accuracy of geometry optimizations (**1** = captopril, **2** = epinephrine, **3** = menthol, **4** = tryptophane, **5** = adenine, and **6** = D-glucose).

a factor of 4 for the TZVPP basis set and ~6 for the QZVP basis set (cf. speedup for the menthol molecule in QZVP basis: with LIBINT package −11.6, without LIBINT package −61.2).

The speedups listed in Table 2 concerning the MP2 energy correction obtained with the RI approximation compared to the conventional MP2 correction generally decrease with larger basis sets. This is caused by the higher angular momenta in the auxiliary basis set and the associated generation of the three-index integrals in the atomic orbital basis. Replacing the QZVP/C auxbasis by the smaller TZVPP/C auxbasis set, i.e., reducing the highest angular momentum from *h* to *g*, yields roughly a speedup of ~35 in the RI-MP2 module compared to that of the conventional MP2 for the adenine molecule in a QZVP orbital basis.

The deviation in total single point energies introduced by the different approximations is on the same order of magnitude with absolute errors amounting to 0.1−0.4 kcal/mol with RI and RIJ-DX. The error for the RIJ-DX approximation is overall negative, which results from the well-known variational nature of Coulomb energy by the RI approximation.[66,67,48] The error in total single point energies introduced by the RIJCOSX approximation is about one order of magnitude larger than what is obtained with RIJ-DX and is overall positive. The errors are larger for the extended QZVP basis set, which has also been reported for the RIJCOSX-HF energy in ref 44. These errors can be reduced by applying a larger Lebedev final grid.

Accuracy of the RIJCOSX-MP2 Gradient. In order to prove the accuracy of the geometries predicted with the RI, RIJ-DX, and RIJCOSX approximations in restricted MP2 (RMP2) calculations, we performed structure optimizations on some representative medium-sized molecules (Figure 4).

In Table 3, deviations of the structural parameters relative to the original MP2 method are collected. The RIJ-DX approximation introduces no noticeable error compared to the original RI-MP2 method. The deviations introduced by the RI approximation are on average ≤0.01 pm in bond distances and 0.005° in bond angles. The maximum absolute errors are 0.03 pm in bond lengths and 0.02° in bond angles. The RIJCOSX approximation introduces deviations, which are about one order of magnitude larger. Bond distances deviate by about 0.1 pm from their parent values, whereas bond angles differ typically by less than 0.2°. The largest

Table 3. Statistical Analysis of Errors in the Optimized Geometries of Molecules 1−6 from the RI, RIJ-DX, and RIJCOSX Approximations Compared to the Parent RMP2 Method[a]

		|Δ mean distances|	|Δ mean absolute distances|	|Δ max distances|	|Δ mean angles|	|Δ mean absolute angles|	|Δ max angles|
1	RI-MP2	−0.011	0.011	0.020	−0.001	0.003	0.020
	RIJ-DX-MP2	−0.013	0.013	0.020	−0.001	0.004	0.020
	RIJCOSX-MP2	−0.001	0.102	0.400	−0.005	0.145	0.400
2	RI-MP2	−0.007	0.007	0.020	0.001	0.002	0.020
	RIJ-DX-MP2	−0.008	0.008	0.030	0.000	0.002	0.010
	RIJCOSX-MP2	−0.031	0.075	0.170	−0.014	0.139	0.380
3	RI-MP2	−0.012	0.012	0.020	0.000	0.001	0.010
	RIJ-DX-MP2	−0.013	0.013	0.030	0.000	0.002	0.010
	RIJCOSX-MP2	−0.036	0.077	0.240	−0.001	0.133	0.400
4	RI-MP2	−0.004	0.004	0.020	0.000	0.002	0.010
	RIJ-DX-MP2	−0.005	0.006	0.020	0.000	0.005	0.010
	RIJCOSX-MP2	−0.001	0.075	0.220	0.001	0.164	0.730
5	RI-MP2	−0.004	0.004	0.020	0.003	0.004	0.020
	RIJ-DX-MP2	−0.004	0.004	0.020	0.003	0.004	0.020
	RIJCOSX-MP2	−0.031	0.044	0.130	0.015	0.073	0.280
6	RI-MP2	−0.006	0.006	0.020	0.000	0.002	0.010
	RIJ-DX-MP2	−0.007	0.007	0.020	0.000	0.002	0.010
	RIJCOSX-MP2	−0.011	0.086	0.310	0.004	0.106	0.360

[a] Errors are given relative to the parent MP2 method. All calculations were done with the TZVP basis set (distances in pm and angles in degrees). *N*(distances) for molecules 1−6 = 30, 26, 31, 38, 16, and 23, *N*(angles) for molecules 1−6 = 56, 42, 61, 46, 24, and 28. Errors in final total energies are for RI = 0.7, 0.3, 0.9, 0.3, 0.1, and 0.2 kcal/mol, RIJ-DX = 0.5, 0.2, 0.7, 0.1, − 0.1, and 0.1 kcal/mol, and RIJCOSX = 0.6, 0.9, 1.6, 0.8, 0.4, and 0.4 kcal/mol.

Table 4. Efficiency of the RIJ-DX and RIJCOSX Algorithms for MP2 Calculations on Medium-Sized Molecules with Different Basis Sets[a]

						speedup		
molecule	N_{atoms}	basis	N_{basis}	$\Delta_{RIJ\text{-}DX}$	$\Delta_{RIJCOSX}$	RI	RIJ-DX	RIJCOSX
adenine	15	SV(P)	150	−0.0001	−0.0009	1.3	1.3	1.3
		TZVP	220	−0.0001	−0.0004	1.4	1.4	2.3
		TZVPP	380	0.0001	−0.0009	1.3	1.3	4.1
cysteine	14	SV(P)	116	−0.0002	−0.0010	1.2	1.2	0.8
		TZVP	178	−0.0002	−0.0013	1.2	1.4	1.7
		TZVPP	318	0.0000	−0.0011	1.4	1.4	3.7
cytosine	13	SV(P)	122	−0.0001	−0.0017	1.2	1.2	1.1
		TZVP	182	−0.0002	−0.0015	1.2	1.4	1.8
		TZVPP	318	0.0001	−0.0016	1.2	1.3	3.6
D-glucose	24	SV(P)	192	0.0004	−0.0001	1.5	1.5	1.2
		TZVP	300	0.0004	0.0002	1.6	1.8	2.8
		TZVPP	540	−0.0002	−0.0002	1.6	2.0	5.6
epinephrine	26	SV(P)	208	0.0000	0.0000	1.4	1.4	1.3
		TZVP	325	0.0002	0.0014	1.6	1.9	3.0
		TZVPP	585	0.0000	0.0011	1.7	1.9	5.6
ferrocene	21	SV(P)	184	−0.0002	−0.0008	1.2	1.3	1.6
		TZVP	283	−0.0005	−0.0012	1.3	1.3	3.0
		TZVPP	490	0.0002	−0.0009	1.3	1.7	5.3
glycine	10	SV(P)	80	−0.0002	−0.0007	1.2	1.0	0.7
		TZVP	125	−0.0003	−0.0002	1.2	1.1	1.1
		TZVPP	225	0.0000	0.0000	1.3	1.2	2.8
guanine	16	SV(P)	164	0.0000	−0.0015	1.4	1.3	1.5
		TZVP	239	0.0000	−0.0017	1.4	1.5	2.5
		TZVPP	411	0.0001	−0.0014	1.3	1.4	4.4
histidine	20	SV(P)	172	−0.0003	−0.0003	1.4	1.3	1.2
		TZVP	263	−0.0003	−0.0002	1.5	1.7	2.6
		TZVPP	467	0.0000	0.0001	1.6	1.8	5.1
menthol	31	SV(P)	194	0.0002	0.0003	1.3	1.6	1.0
		TZVP	329	0.0003	0.0000	1.6	1.8	2.9
		TZVPP	621	0.0002	−0.0001	1.9	2.4	7.5
nitroglycerine	17	SV(P)	178	0.0001	−0.0005	1.4	1.4	1.3
		TZVP	258	0.0001	−0.0002	1.5	1.7	2.9
		TZVPP	442	0.0001	−0.0004	1.5	1.7	5.2
thymine	15	SV(P)	138	0.0000	−0.0008	1.2	1.1	1.0
		TZVP	207	0.0000	−0.0011	1.4	1.4	2.0
		TZVPP	363	0.0001	−0.0012	1.4	1.5	4.3
tyrosine	24	SV(P)	204	−0.0003	−0.0006	1.6	1.6	1.3
		TZVP	313	−0.0002	−0.0006	1.5	1.7	3.0
		TZVPP	557	0.0000	−0.0005	1.6	1.9	5.8

[a] Speedup refers to the ratio of total wall clock times required to finish one gradient calculation. The speedups are given relative to the original MP2 method without any approximations. The deviation of the gradient norm w.r.t. the MP2 reference is denoted $\Delta_{RIJ\text{-}DX}$ and $\Delta_{RIJCOSX}$ in (E_h /bohr).

error in bond lengths is up to 0.4 pm, the corresponding error in bond angles is 0.7°. The mean absolute deviations for the RIJCOSX-MP2 method are in the same range observed previously for the RIJCOSX-HF method.[44] The deviations of the final total energies from the canonical values remain below 2 kcal/mol and are significantly smaller when compared to the RI-MP2 method (<1 kcal/mol).

Efficiency of the RIJCOSX-MP2 Method. In Tables 4 and 5 the efficiency of the RIJ-DX-MP2 and RIJCOSX-MP2 methods is demonstrated compared to the original MP2 as well as to the already very efficient RI-MP2 method.

The speedups listed in Table 4 show the efficiency of the RI, RIJ-DX, and RIJCOSX approximations for 13 medium-sized molecules for 3 different basis sets with up to ∼620 basis functions. The RIJ-DX approximation shows speedups up to a factor of 2.4 in the gradient calculations but represents no major improvement over the original RI approximation. In general, the speedup becomes noticeable for ∼200 basis functions. The speedups tend to become more remarkable with larger basis sets, but the enhancements are almost not observable.

The RIJCOSX approximation shows only minor speedups for the smallest employed basis set SV(P). For the smallest molecules in our test suite, the RIJCOSX approximation even slows down the MP2 gradient calculations. For the next larger basis set TZVP, the RIJCOSX approximation accelerates the calculations by a factor of ∼3 for molecules with around 300 basis functions. The speedup increases noticeably with basis set and system size. In the case of the menthol molecule, a factor of ∼7.5 in computation time is gained, if the RIJCOSX approximation is applied. For comparison, the speedup reduces to ∼4 when RI-MP2 serves as reference.

The deviation of the gradient norm shows a deviation for RIJCOSX-MP2, which is naturally somewhat larger than for the RIJ-DX approximation but as has been shown in the previous subsection, this has almost no influence on the resulting structures.

Table 5. Efficiency of the RIJ-DX and RIJCOSX Algorithms for RI-MP2 Calculations on Medium-Sized Molecules with Different Basis Sets.[a]

						speedup (RIJ-DX)		speedup (RIJCOSX)	
molecule	N_{atoms}	basis	N_{basis}	Δ_{RIJ-DX}	$\Delta_{RIJCOSX}$	RI-MP2	total	RI-MP2	total
adenine	15	SV(P)	150	0.0000	−0.0009	1.0	1.0	1.0	1.0
		TZVP	220	0.0000	−0.0004	1.1	1.0	1.5	1.7
		TZVPP	380	0.0001	−0.0009	1.0	1.0	2.9	3.1
		QZVP	720	0.0001	−0.0010	1.1	1.1	5.9	6.3
beclometahsone	57	SV(P)	454	0.0004	0.0007	1.2	1.2	1.1	1.3
		TZVP	709	0.0003	0.0004	1.3	1.4	2.0	2.5
		TZVPP	1277	0.0000	0.0001	1.2	1.3	2.4	3.3
captopril	30	SV(P)	220	0.0002	0.0008	1.1	1.1	0.8	0.9
		TZVP	352	0.0001	0.0005	1.3	1.3	1.6	2.0
		TZVPP	644	0.0002	0.0006	1.2	1.2	2.9	3.4
		QZVP	1264	0.0002	0.0005	1.4	1.4	4.9	6.2
cholesterole	74	SV(P)	484	0.0004	0.0001	1.1	1.1	1.0	1.1
		TZVP	808	0.0003	−0.0004	1.4	1.4	1.7	2.2
		TZVPP	1512	0.0002	−0.0001	1.4	1.4	2.1	2.9
CO-heme	86	SV(P)	782	0.0000	−0.0001	1.2	1.2	1.1	1.3
		TZVP	1180	0.0000	−0.0002	1.2	1.3	1.6	2.2
cysteine	14	SV(P)	116	−0.0002	−0.0009	1.0	1.0	0.6	0.7
		TZVP	178	−0.0002	−0.0013	1.2	1.2	1.2	1.3
		TZVPP	318	0.0000	−0.0011	1.0	1.0	2.6	2.7
		QZVP	622	0.0000	−0.0010	1.2	1.2	5.1	5.5
cytosine	13	SV(P)	122	−0.0001	−0.0016	1.0	1.0	0.8	0.9
		TZVP	182	−0.0002	−0.0014	1.1	1.2	1.4	1.5
		TZVPP	318	0.0001	−0.0016	1.0	1.0	2.7	2.9
		QZVP	606	0.0001	−0.0016	1.1	1.1	5.6	6.0
D-glucose	24	SV(P)	192	0.0003	−0.0002	1.0	1.0	0.8	0.8
		TZVP	300	0.0003	0.0001	1.1	1.1	1.4	1.7
		TZVPP	540	−0.0002	−0.0002	1.3	1.3	3.1	3.6
		QZVP	1044	0.0000	−0.0002	1.4	1.3	4.5	5.5
dibenzo-crown-18-6	50	SV(P)	412	−0.0001	0.0000	1.2	1.2	1.0	1.1
		TZVP	638	0.0003	0.0001	1.3	1.3	1.6	2.0
		TZVPP	1142	0.0002	0.0000	1.3	1.3	2.1	2.7
epinephrine	26	SV(P)	208	−0.0001	0.0000	1.1	1.0	0.9	0.9
		TZVP	325	0.0002	0.0014	1.2	1.2	1.5	1.8
		TZVPP	585	0.0000	0.0011	1.1	1.1	2.7	3.4
		QZVP	1131	0.0000	0.0008	1.4	1.4	5.2	6.7
ferrocene	21	SV(P)	184	−0.0001	−0.0007	1.1	1.1	1.4	1.3
		TZVP	283	−0.0005	−0.0012	1.1	1.0	2.0	2.4
		TZVPP	490	0.0003	−0.0009	1.0	1.3	3.5	4.0
		QZVP	954	0.0003	−0.0020	1.0	1.0	4.5	5.7
flutamide	30	SV(P)	288	0.0004	0.0016	1.1	1.1	1.0	1.1
		TZVP	427	0.0001	0.0014	1.2	1.2	1.6	2.0
		TZVPP	743	0.0000	0.0013	1.1	1.1	2.5	3.0
		QZVP	1413	0.0000	0.0013	1.4	1.4	4.5	5.8
glycine	10	SV(P)	80	−0.0002	−0.0007	0.8	0.9	0.5	0.6
		TZVP	125	−0.0002	−0.0002	1.0	0.9	0.9	0.9
		TZVPP	225	0.0000	0.0000	1.0	0.9	2.2	2.2
		QZVP	435	0.0000	−0.0003	1.1	1.0	4.6	4.7
guanine	16	SV(P)	164	0.0001	−0.0013	0.9	0.9	1.0	1.1
		TZVP	239	0.0001	−0.0015	1.1	1.1	1.6	1.8
		TZVPP	411	0.0001	−0.0013	1.0	1.0	3.1	3.3
		QZVP	777	0.0001	−0.0017	1.2	1.2	5.9	6.6
histidine	20	SV(P)	172	−0.0002	−0.0002	0.9	0.9	0.8	0.9
		TZVP	263	−0.0002	−0.0001	1.1	1.1	1.4	1.7
		TZVPP	467	0.0001	0.0001	1.2	1.1	2.8	3.2
		QZVP	897	0.0000	0.0001	1.3	1.2	5.3	6.2
menthol	31	SV(P)	194	0.0001	0.0002	1.2	1.2	0.6	0.7
		TZVP	329	0.0003	0.0000	1.3	1.1	1.5	1.8
		TZVPP	621	0.0001	−0.0002	1.3	1.2	3.2	3.9
		QZVP	1227	0.0000	0.0001	1.4	1.4	5.3	7.3
morphin	40	SV(P)	332	0.0001	0.0002	1.2	1.2	1.3	1.4
		TZVP	513	0.0001	0.0005	1.3	1.2	2.3	2.9
		TZVPP	917	0.0001	0.0008	1.3	1.3	3.1	4.2
		QZVP	1767	0.0001	0.0004	1.3	1.3	5.1	7.0
NiTrenNCS2	35	SV(P)	292	0.0000	0.0006	1.1	1.1	1.3	1.5
		TZVP	451	0.0001	0.0005	1.1	1.4	1.7	2.6
		TZVPP	794	0.0000	0.0002	1.3	1.3	2.9	4.0
		QZVP	1562	0.0000	0.0005	1.4	1.4	5.1	9.2
nitroglycerine	17	SV(P)	178	0.0001	−0.0005	1.1	1.0	0.9	0.9
		TZVP	258	0.0001	−0.0002	1.1	1.1	1.7	1.9

Table 5 Continued

molecule	N_{atoms}	basis	N_{basis}	Δ_{RIJ-DX}	$\Delta_{RIJCOSX}$	speedup (RIJ-DX) RI-MP2	speedup (RIJ-DX) total	speedup (RIJCOSX) RI-MP2	speedup (RIJCOSX) total
		TZVPP	442	0.0001	−0.0004	1.1	1.1	3.0	3.4
		QZVP	834	0.0001	−0.0003	1.3	1.2	4.8	5.6
penicilin	42	SV(P)	376	0.0000	0.0007	1.1	1.1	1.1	1.2
		TZVP	567	0.0001	−0.0002	1.2	1.2	1.6	1.9
		TZVPP	999	0.0001	0.0010	1.3	1.3	2.3	2.9
		QZVP	1921	0.0001	0.0007	1.5	1.5	3.6	4.7
tetracycline	56	SV(P)	496	0.0001	0.0019	1.2	1.2	1.2	1.4
		TZVP	752	0.0001	0.0022	1.2	1.3	1.8	2.2
		TZVPP	1328	0.0000	0.0019	1.2	1.3	2.2	2.9
thymine	15	SV(P)	138	0.0000	−0.0007	0.9	0.9	0.8	0.8
		TZVP	207	0.0001	−0.0011	1.0	1.0	1.3	1.5
		TZVPP	363	0.0001	−0.0012	1.1	1.1	2.2	2.9
		QZVP	693	0.0001	−0.0014	1.1	1.1	5.3	5.8
tryptophane	27	SV(P)	234	−0.0002	0.0000	1.1	1.1	1.0	1.1
		TZVP	357	−0.0002	−0.0001	1.1	1.1	1.6	2.0
		TZVPP	633	0.0001	0.0001	1.2	1.2	2.9	3.6
		QZVP	1215	0.0001	0.0000	1.4	1.4	5.2	6.7
tyrosine	24	SV(P)	204	−0.0003	−0.0006	1.0	1.0	0.8	0.9
		TZVP	313	−0.0002	−0.0006	1.1	1.1	1.7	1.9
		TZVPP	557	0.0000	−0.0004	1.1	1.1	3.1	3.6
		QZVP	1071	0.0000	−0.0003	1.3	1.3	4.8	5.9

[a] Speedup refers to the ratio of wall clock times of either the RI-MP2 module (RI-MP2) or the total wall clock time (total) required to finish one gradient calculation. The deviation of the gradient norm w.r.t. the RI-MP2 reference is denoted Δ_{RIJ-DX} and $\Delta_{RIJCOSX}$ in (E_h /bohr).

In Table 5 the speedup of the RIJ-DX and RIJCOSX approximations to the MP2 gradient is related to the very efficient RI-MP2 gradient. Therefore, we studied 24 molecules in the range of 10−86 atoms with ∼100−1900 basis functions. The speedup obtained with the RIJ-DX-MP2 method compared to RI-MP2 is about a factor of ∼1.2. The inclusion of the SCF wall clock time has almost no consequence on the overall speedup.

For the smallest basis set in our test set SV(P), the speedup for the RIJCOSX approximation in the MP2 module is almost negligible, and the inclusion of the SCF wall clock times has no influence on the entire performance. The speedup of the RIJCOSX approximation becomes more observable for the triple-ζ basis set TZVP and for molecules with ≥300 basis functions (∼1.5−2.3).

For the TZVPP basis set, the speedup varies from a factor of 2−3 for the MP2 module, and even reaches a factor of 4.2 for the morphin molecule when the SCF calculation is taken into account. Excellent speedups are obtained with the more extended QZVP basis set. Speedups of a factor ∼4.5−6 are obtained for the MP2 module, and even a factor of 9.2 is achieved for the NiTrenNCS2 molecule when the SCF wall clock time is included in the comparison. This behavior has to be expected due to the favorable scaling of the RIJCOSX approximation with respect to higher angular momenta.

In order to verify the quality of the calculated gradients, we also listed the errors in the norm of the MP2 gradient in Table 5.

Timing Analysis of the RIJCOSX-MP2 Method. A detailed analysis of the timings for the different parts of the MP2 gradient is presented in this subsection. For the comparison of the original MP2 with the RIJCOSX-MP2 method, the menthol molecule in a TZVPP basis serves as an example. The calculation of one MP2 gradient takes about ∼18 h. The time spent in the MP2 module is ∼14 h (80% of the total wall clock time).

Table 6. Timings in (s) of the Individual Contributions to the MP2 Gradient[a]

gradient components	MP2	RI-MP2	RIJ-DX-MP2	RIJCOSX-MP2
integral transformation	18 061	133	129	136
K^{ij}(a,b)	65	145	144	148
T^{ij}(a,b)	27	17	16	17
D(virtual)	60	61	60	60
D(internal)	1537	124	117	122
W(virtual)	120	121	119	121
W(internal)	191	217	194	201
L(3-ext)	1510	260	250	257
L(3-int)	16	6	6	6
R(*D*)	1170	1209	949	146
R(Z)	1209	1213	969	148
Z-vector solution	5410	5497	4062	773
separable gradient (S)		10918	8937	3733
nonseparable gradient (NS)		582	325	327
gradient (S + NS)	20 290	11 500	9262	4060
total time	49 689	20 732	16 533	6460

[a] Depending on the employed approximation obtained for the menthol molecule (31 atoms) in a TZVPP basis set.

A detailed analysis of the different components of the MP2 gradient is given in Table 6. The integral transformation in the original MP2 method corresponds to a three-fourths transformation of AO integrals to the molecular orbital (MO) basis, and the calculation of separable and nonseparable gradient contributions is the most time-consuming step. The evaluation of the internal part of the unrelaxed density matrix **D**(internal) is more expensive than in the RI-MP2 variants due to the generation of the required integrals containing one frozen-core index on the fly. The formation of the three-external part of the Lagrangian L(3-ext), eq 23 is also more costly in terms of computation time due to the large AO↔MO transformations. The calculation of the nonseparable and separable gradient, eq 18, is done simultaneously

in the original MP2 code, and the time-determining step is the calculation of the derivative of the two-electron repulsion integrals.

The situation changes drastically when going to the RI-MP2 variants. The time required for the integral transformation is negligible, since in RI-MP2 methods only three-index integrals are needed, which can be calculated very efficiently. The formation of the exchange integrals becomes somewhat more expensive due to the larger matrix multiplications, but the effect on the overall timing is insignificant. The evaluation of **D**(internal) is more effcient due to prestored frozen-core integrals, and the three-external part of the Lagrangian only requires the transformation of one virtual index. The calculation of the separable gradient is done analogously to the parent MP2 method, but the nonseparable part is very efficiently calculated employing three- and two-index derivative integrals, eq 30.

The speedup achieved with the RIJ-DX approximation results from the more efficient calculation of the response-type operators and, as a consequence, the accelerated solution of the z-vector equations. The separable gradient profits from the application of the RI approximation to the Coulomb contribution, whereas the nonseparable gradient saves computation time through storage of the three-index/two-particle density and the use of large BLAS level two operations.

The RIJCOSX approximation introduces a highly efficient treatment of the exchange-type contributions to the MP2 gradient. The calculation of the response-type operators, eq 32, and the solution of the z-vector equations is highly dominated by the formation of the exchange-type contributions. The employment of the RIJCOSX approximation speeds the calculation of these contributions up by a factor of $\sim$7−8. A speedup of $\sim$2 is gained by exploiting the efficient calculation of the basis function derivatives on the grid, as ingredient to the separable gradient.

Parallelization. The separable COSX-MP2 gradient, eq 29, is parallelized over batches of grid points. A reasonable load balancing is achieved by distributing the batches of grid points over the processors such that all processors work on all parts of the molecular system to nearly the same extent. A single gather operation is then performed at the end of the COSX integration loop, in order to keep the communication overhead negligible. The same strategy has been followed for the parallel exchange treatment in the SCF module.

In Figure 5 the efficiency of the parallel implementation is demonstrated for a medium-sized molecule (dibenzo-crown-18-6/QZVP, 50 atoms, 2202 basis functions). The scaling behavior is excellent for up to 16 processors, although the example is not really large. However, the evaluation of the basis function derivatives on the grid requires the large Lebedev-302 angular grid with an integration accuracy of 4.34, which yields about 185 000 grid points that are divided among the processors. Some of the plotted speedups in Figure 5 seem to be better than the linear speedup, which is mainly due to the inaccuracy in the time measurement, since no statistics have been performed.

The parallelization of the entire MP2 gradient module, presented in Figure 6, is less efficient than that for the separable COSX-MP2 gradient contribution. However, for up to at least 10 processors reasonable speedups are achieved. The reason for the apparent stagnation of the speedup with 12 processors is the poor scaling of the three-external part to the MP2 Lagrangian and of the separable gradient calculated in the RI approximation with the number of processors employed. The speedup of the evaluation of the three-external Lagrangian contribution achieves a factor 4.4 for 10 processors and decreases to a factor of 3.8 for 12 and 16 processors. A similar situation is found for the separable gradient calculated within the RI approximation. Although not rate determining, the speedup amounts to only a factor of $\sim$3. The scaling of the internal part of the energy weighted density matrix is also reduced to a factor of 10 for 16 processors. All three contributions together determine 30% of the total wall clock time needed for the calculation on 16 processors. Furthermore, some smaller parts of the parallel MP2 gradient do not scale ideally with the number of used processors. Taken together, these factors are responsible for the worsened scaling starting with 10−12 employed processors.

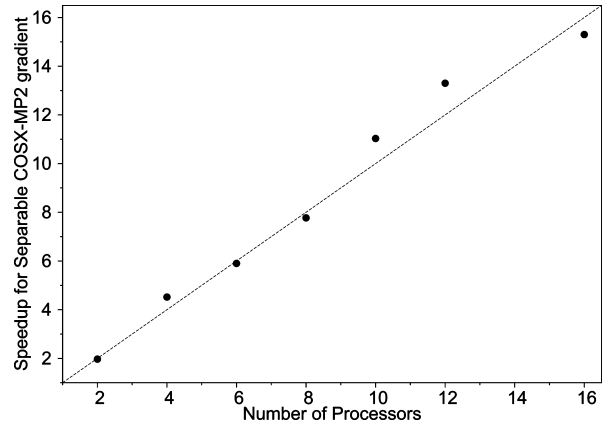

Figure 5. Parallelization efficiency of the COSX gradient algorithm with dibenzo-crown-18-6/QZVP as an example. Plotted is the wall clock time required for formation of the entire separable COSX-MP2 gradient relative to the time taken for the same operation by a single process.

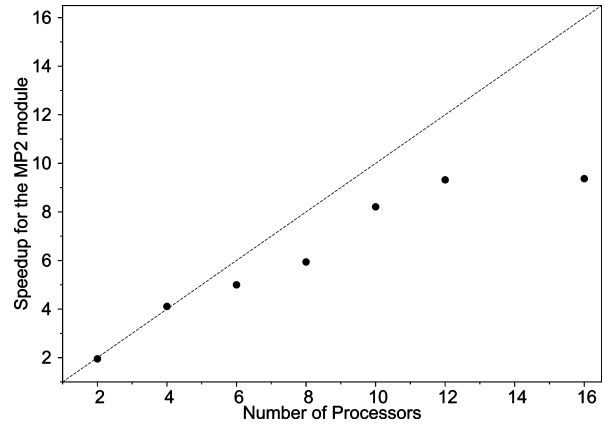

Figure 6. Parallelization efficiency of the MP2 gradient algorithm with dibenzo-crown-18-6/QZVP as an example. Plotted is the wall clock time required for formation of the entire COSX-MP2 gradient relative to the time taken for the same operation by a single process.

Discussion

In the present work, the applicability of the seminumeric exchange treatment via the COSX approximation to the exchange-type contributions of the MP2 gradient has been reported. The entire RIJCOSX-MP2 gradient algorithm fulfills all important requirements required by a reliable approximate method. The optimized structures show only negligible deviations from the MP2 structures. The RIJ-COSX-MP2 gradient is efficient with observed speedups in wall clock times of ∼7−7.5 for the TZVPP basis set compared to conventional MP2 regarding one gradient calculation (including the SCF time). RIJCOSX-MP2 versus RI-MP2 yields also speedups of ∼5−9 for one entire energy and gradient calculation with the QZVP basis.

The RIJCOSX-MP2 method is generally applicable and does neither depend on the molecular system nor on the chosen basis set. The program is parallelized and scales reasonably well with the number of used processors, but some more work is required before efficient large-scale parallelization on many processors is achieved. Overall, we believe that the present development adds to the applicability of MP2-type methods, such as MP2, SCS-MP2, or double hybrid density functional theory in large-scale chemical applications. The method is implemented in the freely available ORCA program.

References

(1) Møller, C.; Plesset, M. S. *Phys. Rev.* **1934**, *46*, 618–622.

(2) Brillouin, L. *Actual. Sci. Ind.* **1934**, *71*, 159.

(3) Grimme, S. *J. Chem. Phys.* **2003**, *118*, 9095–9102.

(4) Gerenkamp, M.; Grimme, S. *Chem. Phys. Lett.* **2004**, *392*, 229–235.

(5) Jung, Y. S.; Lochan, R. C.; Dutoi, A. D.; Head-Gordon, M. *J. Chem. Phys.* **2004**, *121*, 9793–9802.

(6) Lochan, R. C.; Head-Gordon, M. *J. Chem. Phys.* **2007**, *126*, 164101.

(7) Jung, Y. S.; Shao, Y.; Head-Gordon, M. *J. Comput. Chem.* **2007**, *28*, 1953–1964.

(8) Grimme, S. *J. Chem. Phys.* **2006**, *124*, 034108.

(9) Neese, F.; Schwabe, T.; Grimme, S. *J. Chem. Phys.* **2007**, *126*, 124115.

(10) Saebø, S.; Almlöf, J. *Chem. Phys. Lett.* **1989**, *154*, 83–89.

(11) Head-Gordon, M.; Pople, J. A.; Frisch, M. J. *Chem. Phys. Lett.* **1988**, *153*, 503–506.

(12) Haase, F.; Ahlrichs, R. *J. Comput. Chem.* **1993**, *14*, 907–912.

(13) Saebø, S.; Pulay, P. *J. Chem. Phys.* **2001**, *115*, 3975–3983.

(14) Baker, J.; Pulay, P. *J. Comput. Chem.* **2002**, *23*, 1150–1156.

(15) Saebø, S.; Baker, J.; Wolinski, K.; Pulay, P. *J. Chem. Phys.* **2004**, *120*, 11423–11431.

(16) Ishimura, K.; Pulay, P.; Nagase, S. *J. Comput. Chem.* **2006**, *27*, 407–413.

(17) Baker, J.; Wolinski, K.; Malagoli, M.; Kinghorn, D.; Wolinski, P.; Magyarfalvi, G.; Saebø, S.; Janowski, T.; Pulay, P. *J. Comput. Chem.* **2008**, *30*, 317–335.

(18) Almlöf, J. *Chem. Phys. Lett.* **1991**, *181*, 319–320.

(19) Häser, M.; Almlöf, J. *J. Chem. Phys.* **1992**, *96*, 489–494.

(20) Häser, M. *Theor. Chim. Acta* **1993**, *87*, 147–173.

(21) Ayala, P. Y.; Kudin, K. N.; Scuseria, G. E. *J. Chem. Phys.* **2001**, *115*, 9698–9707.

(22) Lambrecht, D. S.; Doser, B.; Ochsenfeld, C. *J. Chem. Phys.* **2005**, *123*, 184102.

(23) Doser, B.; Lambrecht, D. S.; Ochsenfeld, C. *Phys. Chem. Chem. Phys.* **2008**, *10*, 3335–3344.

(24) Schweizer, S.; Doser, B.; Ochsenfeld, C. *J. Chem. Phys.* **2008**, *128*, 154101.

(25) Doser, B.; Lambrecht, D. S.; Kussmann, J.; Ochsenfeld, C. *J. Chem. Phys.* **2009**, *130*, 064107.

(26) Rauhut, G.; Pulay, P.; Werner, H. J. *J. Comput. Chem.* **1998**, *19*, 1241–1254.

(27) El Azhary, A.; Rauhut, G.; Pulay, P.; Werner, H. J. *J. Chem. Phys.* **1998**, *108*, 5185–5193.

(28) Hetzer, G.; Schütz, M.; Stoll, H.; Werner, H. J. *J. Chem. Phys.* **2000**, *113*, 9443–9455.

(29) Werner, H. J.; Manby, F. R.; Knowles, P. J. *J. Chem. Phys.* **2003**, *118*, 8149–8160.

(30) Schütz, M.; Werner, H. J.; Lindh, R.; Manby, F. R. *J. Chem. Phys.* **2004**, *121*, 737–750.

(31) Saebø, S.; Pulay, P. *Chem. Phys. Lett.* **1985**, *113*, 13–18.

(32) Saebø, S.; Pulay, P. *Annu. Rev. Phys. Chem.* **1993**, *44*, 213–236.

(33) Pulay, P. *Chem. Phys. Lett.* **1983**, *100*, 151–154.

(34) Kendall, R. A.; Früchtl, H. A. *Theor. Chim. Acta* **1997**, *97*, 158–163.

(35) Feyereisen, M.; Fitzgerald, G.; Komornicki, A. *Chem. Phys. Lett.* **1993**, *208*, 359–363.

(36) Vahtras, O.; Almlöf, J.; Feyereisen, M. W. *Chem. Phys. Lett.* **1993**, *213*, 514–518.

(37) Pople, J. A.; Krishnan, R.; Schlegel, H. B.; Binkley, J. S. *Int. J. Quantum Chem.* **1979**, *16*, 225–241.

(38) Frisch, M. J.; Head-Gordon, M.; Pople, J. A. *Chem. Phys. Lett.* **1990**, *166*, 275–280.

(39) Frisch, M. J.; Head-Gordon, M.; Pople, J. A. *Chem. Phys. Lett.* **1990**, *166*, 281–289.

(40) Weigend, F.; Häser, M. *Theor. Chem. Acc.* **1997**, *97*, 331–340.

(41) Rhee, Y. M.; DiStasio, R. A.; Lochan, R. C.; Head-Gordon, M. *Chem. Phys. Lett.* **2006**, *426*, 197–203.

(42) DiStasio, R. A.; Steele, R. P.; Rhee, Y. M.; Shao, Y.; Head-Gordon, M. *J. Comput. Chem.* **2007**, *28*, 839–856.

(43) Simandiras, E. D.; Handy, N. C.; Amos, R. D. *Chem. Phys. Lett.* **1987**, *133*, 324–330.

(44) Neese, F.; Wennmohs, F.; Hansen, A.; Becker, U. *Chem. Phys.* **2009**, *356*, 98–109.

(45) Handy, N. C.; Schaefer, H. F., III *J. Chem. Phys.* **1984**, *81*, 5031–5033.

(46) Becke, A. D. *J. Chem. Phys.* **1988**, *88*, 2547–2553.

(47) Ko, C.; Malick, D. K.; Braden, D. A.; Friesner, R. A.; Martinez, T. J. *J. Chem. Phys.* **2008**, *128*, 104103.

(48) Eichkorn, K.; Treutler, O.; Öhm, H.; Häser, M.; Ahlrichs, R. *Chem. Phys. Lett.* **1995**, *242*, 652–660.

(49) Eichkorn, K.; Weigend, F.; Treutler, O.; Ahlrichs, R. *Theor. Chem. Acc.* **1997**, *97*, 119–124.

(50) Neese, F. *J. Comput. Chem.* **2003**, *24*, 1740–1747.

(51) Neese, F.; Becker, U.; Ganyushin, D.; Koβmann, S.; Hansen, A.; Liakos, D.; Petrenko, T.; Riplinger, C.; Wennmohs, F. *ORCA*, version 2.7.0; University of Bonn: Bonn, Germany, 2009.

(52) Schäfer, A.; Horn, H.; Ahlrichs, R. *J. Chem. Phys.* **1992**, *97*, 2571–2577.

(53) Schäfer, A.; Huber, C.; Ahlrichs, R. *J. Chem. Phys.* **1994**, *100*, 5829–5835.

(54) Weigend, F.; Furche, F.; Ahlrichs, R. *J. Chem. Phys.* **2003**, *119*, 12753–12762.

(55) Ahlrichs, R.; Furche, F.; Hättig,C.; Klopper, W. M.; Sierka, M.; Weigend, F. *TurboMole basis set library*; TURBOMOLE GmbH: Karlsruhe, Germany; ftp.chemie.uni-karlsruhe.de/pub/BASES (accessed June 24, 2010).

(56) Weigend, F. *Phys. Chem. Chem. Phys.* **2006**, *8*, 1057–1065.

(57) Weigend, F.; Häser, M.; Patzelt, H.; Ahlrichs, R. *Chem. Phys. Lett.* **1998**, *294*, 143–152.

(58) Weigend, F.; Köhn, A.; Hättig, C. *J. Chem. Phys.* **2002**, *116*, 3175–3183.

(59) Hättig, C. *Phys. Chem. Chem. Phys.* **2005**, *7*, 59–66.

(60) Hellweg, A.; Hättig, C.; Hoefener, S.; Klopper, W. *Theor. Chim. Acta* **2007**, *117*, 587–597.

(61) Weigend, F. *J. Comput. Chem.* **2008**, *29*, 167–175.

(62) Aikens, C. M.; Webb, S. P.; Bell, R. L.; Fletcher, G. D.; Schmidt, M. W.; Gordon, M. S. *Theor. Chim. Acta* **2003**, *110*, 233–253.

(63) Krack, M.; Köster, A. M. *J. Chem. Phys.* **1998**, *108*, 3226–3234.

(64) Gill, P. M.-W.; Johnson, B. G.; Pople, J. A. *Chem. Phys. Lett.* **1993**, *209*, 506–512.

(65) Valeev E. ; Fermann J. T. LIBINT integral library; Virginia Tech University: Blacksburg, VA; http://www.files.chem.vt.edu/chem-dept/valeev/software/libint/download.html (accessed June 24, 2010).

(66) Whitten, J. L. *J. Chem. Phys.* **1973**, *58*, 4496–4501.

(67) Dunlap, B. I.; Connolly, J. W. D.; Sabin, J. R. *J. Chem. Phys.* **1979**, *71*, 3396–3402.

CT100199K